Cell, Vol. 121, 633–644, May 20, 2005, Copyright ©2005 by Elsevier Inc. DOI 10.1016/j.cell.2005.04.008

Mechanism of Nodal Flow: A Conserved Symmetry Breaking Event in Left-Right Axis Determination

Yasushi Okada,[1] Sen Takeda,[1] Yosuke Tanaka,[1] Juan-Carlos Izpisúa Belmonte,[2] and Nobutaka Hirokawa[1,*]

[1]Department of Cell Biology and Anatomy
Graduate School of Medicine
University of Tokyo
7-3-1 Hongo
Tokyo, 113-0033
Japan

[2]Gene Expression Laboratory
Salk Institute for Biological Studies
10010 North Torrey Pines Road
La Jolla, California 92037

Summary

The leftward flow in extraembryonic fluid is critical for the initial determination of the left-right axis of mouse embryos. It is unclear if this is a conserved mechanism among other vertebrates and how the directionality of the flow arises from the motion of cilia. In this paper, we show that rabbit and medakafish embryos also exhibit a leftward fluid flow in their ventral nodes. In all cases, primary monocilia present a clockwise rotational-like motion. Observations of defective ciliary dynamics in mutant mouse embryos support the idea that the posterior tilt of the cilia during rotational-like beating can explain the leftward fluid flow. Moreover, we show that this leftward flow may produce asymmetric distribution of exogenously introduced proteins, suggesting morphogen gradients as a subsequent mechanism of left-right axis determination. Finally, we experimentally and theoretically characterize under which conditions a morphogen gradient can arise from the flow.

Introduction

Symmetry breakdown of an egg or body axis determination is one of the fundamental processes of development. Molecules that show left-right (L-R) asymmetric expression in early developmental stages and those that are considered to play important functions in the L-R body axis determination are widely conserved among vertebrates (Bisgrove and Yost, 2001; Mercola and Levin, 2001). However, it remains unclear how the L-R body axis is first determined. This problem is more complex than the determination of the other two axes: anterioposterior (A-P) and dorsoventral (D-V) axes. The L-R axis should be correctly oriented according to the preceding A-P and D-V axes. The mechanism that enables this coordination is unknown. A hypothetical chiral molecule "F" has been proposed to enable this coordination, if the F molecules are aligned in cells with respect to the A-P and D-V axes (Brown and Wolpert, 1990). Although this conceptual proposal is widely accepted, it is unknown how it is actually implemented.

For a number of years, the role of cilia in development and disease has become an all-important issue. Our previous contributions to this topic have demonstrated that the initial event of the L-R body axis determination in a mouse embryo depends on the rotation-like movement of cilia of cells on the ventral surface of the embryonic node (Hirokawa, 2000). Rapid leftward flow of extraembryonic fluid was shown to be critical for correct determination of the L-R axis (Nonaka et al., 1998; Okada et al., 1999; Supp et al., 1999; Takeda et al., 1999; Nonaka et al., 2002). However, the question of how the directionality of the flow is determined remains unanswered. The primary cilia on the node lack the central pair microtubules (Bellomo et al., 1996) and move with rotation-like dynamics (Nonaka et al., 1998; Okada et al., 1999) instead of beating in the plane determined by the central pair microtubules (Wargo and Smith, 2003). The unidirectional flow produced from the vortical rotation-like movement of the cilia requires a specific mechanism, because the simple circling movement of cilia will only produce a vortex in the node. Furthermore, yet another mechanism is required for the conversion of the flow into L-R asymmetric gene expression. In this respect, the formation of morphogen gradients and the asymmetrical bending of mechanoreceptor cilia have been proposed (Nonaka et al., 1998; Okada et al., 1999; McGrath et al., 2003; Tabin and Vogan, 2003).

To elucidate these mechanisms, we compared various vertebrate embryos, with the hypothesis that the basic mechanism is conserved. Essner et al. reported that an embryonic organ with monociliated cells transiently emerges in the various vertebrate embryos (Essner et al., 2002). However, they failed to show whether the cilia move or whether the fluid in the organ flows and how these processes might occur. Since the overall morphology of the embryo, especially the shape around the ventral node, might affect the flow (Nonaka et al., 1998; Okada et al., 1999; Vogan and Tabin, 1999), we compared three differently shaped vertebrate embryos: the mouse egg cylinder (curved with ventral side out), the rabbit embryonic disc (flat), and the medakafish embryo (ventral side in).

In this paper, we report that ventral nodes, covered with cells that have rapidly rotating cilia, transiently develop in embryos of all these three species of vertebrates. Observation of cilia with high spatiotemporal resolution revealed the hydrodynamic mechanism that produces the laminar leftward flow from these rotating cilia. Finally, examination of the distribution of caged fluorescently labeled protein after its local photoactivation demonstrated that this flow produces the concentration gradient of the protein when its molecular weight is about 15–50 kDa. These results are all consistent with the theoretical and in silico studies of the hydrodynamic natures of cilia and the flow induced by the ciliary movement (J. Buceta, M. Ibañes, D. Rasskin-Gutman, Y.O., N.H., and J.-C.I.B., unpublished data),

*Correspondence: hirokawa@m.u-tokyo.ac.jp

and the combination of the experimental and theoretical studies revealed the conserved mechanism that breaks L-R symmetry in vertebrate embryos.

Results and Discussion

Leftward Flow of Extraembryonic Fluid in Ventral Nodes Is Conserved among Various Vertebrate Embryos

To examine the generality of the flow-based mechanism, we observed the ventral surface of early embryos of various species of vertebrates. As a model of the lowest vertebrate, we chose medakafish because of its availability and the size and transparency of the embryo. We also used the rabbit embryo as a model of higher mammals, as it is accepted that the development of the rabbit embryo much resembles that of the human embryo, and therefore it is widely used as a developmental model of humans. For example, at the gastrulation stage, the rabbit develops a planar embryonic disc quite similar to that of a human.

A survey by electron and enhanced video microscopes confirmed that medakafish, rabbit, and mouse embryos develop ventral nodes on their ventral side just before L-R axis determination. This ventral node in the mouse is the nodal pit, while it is the posterior widening of the notochordal plate in the rabbit and Kupffer's vesicle in the medakafish. They are the orthologous organs as described below, and here we use the same name, "ventral node," to refer to these evolutionarily conserved organs to avoid unnecessary confusion.

As we have previously observed with mouse embryos, the cilia in rabbit and medakafish embryos also showed rapid clockwise rotation-like motion, and the fluid in these organs flowed to the left (see Movies S1–S5 in the Supplemental Data available with this article online). However, the shape of the ventral node and the velocity of the flow were significantly different among these three embryos (Figures 1 and 2).

The ventral node of the mouse is a small triangular pit just ventral to the embryonic (dorsal) node (Figures 1A–1C). The fluid in this concave organ flows leftward across the midline just above ($\sim$5 μm) the surface, goes upward along the left sidewall, and then finally returns to the right side by slow counterflow $\sim$20 μm above the surface (Figures 2A, 2D, and 2E; Movie S1). The ventral surface of the notochordal plate, a groove-like structure just anterior to the nodal pit, is also coated with monociliated cells, but the cilia on the notochordal plate are immotile, and the fluid there does not flow in mouse embryos.

However, no ciliated cells were found on the ventral side of the Hensen's node of rabbit embryos. Instead, the monocilia on the notochordal plate moved with similar rotation-like dynamics as described previously in mouse embryos and produced flow in the groove of the notochordal plate (Figures 1D–1H, 2B, and 2F; Movies S2, S3, and S7). The cilia lacked the central pair microtubules and took the so-called 9+0 structure (Figure 1F, inset). The expression of *nodal*, a well-conserved molecular marker for the ventral node (Lowe et al., 1996), on the right and left edges of the notochordal plate (Figures 1E and 1H) indicates that this groove corresponds to the nodal pit of the mouse embryo. The shape of the notochordal plate of the rabbit was very different from that of the murine nodal pit. The surface of the groove-like notochordal plate of the rabbit was convex as evident from the transverse section (Figure 1H). The cilia were the most active on the ridge at the midline, and the cilia on the left and right furrows moved more slowly and intermittently. The fluid flowed rapidly to the left crossing over the midline and then stagnated in the left furrow (Movies S2 and S3). The fluid finally returned to the right side by the slow rightward counter flow at the posterior end of the notochordal plate (Figure 2B, Movie S3).

Similarly, Kupffer's vesicle of the medakafish embryo, the ventral node orthologous to the murine nodal pit (Essner et al., 2002; Amack and Yost, 2004), has a convex monociliated surface (Figures 1I–1L). The cilia lacked the central pair microtubules and took the so-called 9+0 structure (Figure 1L, inset). The fluid in this round-shaped organ crossed the midline by a fast leftward flow produced by the rapidly moving monocilia with rotational-like dynamics, stagnated in the left furrow, and then finally returned to the right furrow by the slow rightward counter flow at the posterior end of Kupffer's vesicle, as observed with rabbit embryos (Figures 2C and 2G, Movies S4 and S5).

Rotation-Like, Nonplanar Beating of Posteriorly Tilted Cilia Produces the Leftward Laminar Flow

How is this fast leftward flow generated from the motion of cilia in the ventral node? The shape of the ventral node does not seem to be an essential factor (Vogan and Tabin, 1999), as evidenced by the existence of a leftward flow in notochordal groove of the rabbit and Kupffer's vesicle of medakafish. Moreover, theoretical and in silico studies also disregard such a possibility (Cartwright et al., 2004; J. Buceta, M. Ibañes, D. Rasskin-Gutman, Y.O., N.H., and J.-C.I.B., unpublished data). Therefore, the mechanism that produces the leftward flow might lie in the movement of cilia. Since the circling movement of the cilia is too fast (10 Hz) for conventional video recording (30 frames per s), we used a high-speed recording system (500 frames per s). The high time resolution video sequence confirmed our previous result in mouse embryos. Unlike other moving cilia—for example, the ones lying on the airway epithelium—where a fast effective stroke is followed by a slow recovery stroke with a planar or half-teardrop-like trajectory (Blake and Sleigh, 1974), the motile monocilia in the node exhibit, as previously reported, a clockwise rotational-like motion with an elliptic or circular trajectory when observed from above (Figures 3A–3C, Movies S6–S8). Interestingly, a more careful inspection reveals that cilia swing almost perpendicular to the apical surface of the nodal pit cell and then sweep back almost parallel just above the apical surface, thus moving around an axis tilted toward the posterior. This motion was most evident with the oblique side view of the ventral node of the medakafish (Movie S9).

For further quantitative description of this posteriorly tilted rotation-like beating of nodal cilia, we analyzed the trajectory of the tip of the cilium. The trajectory is

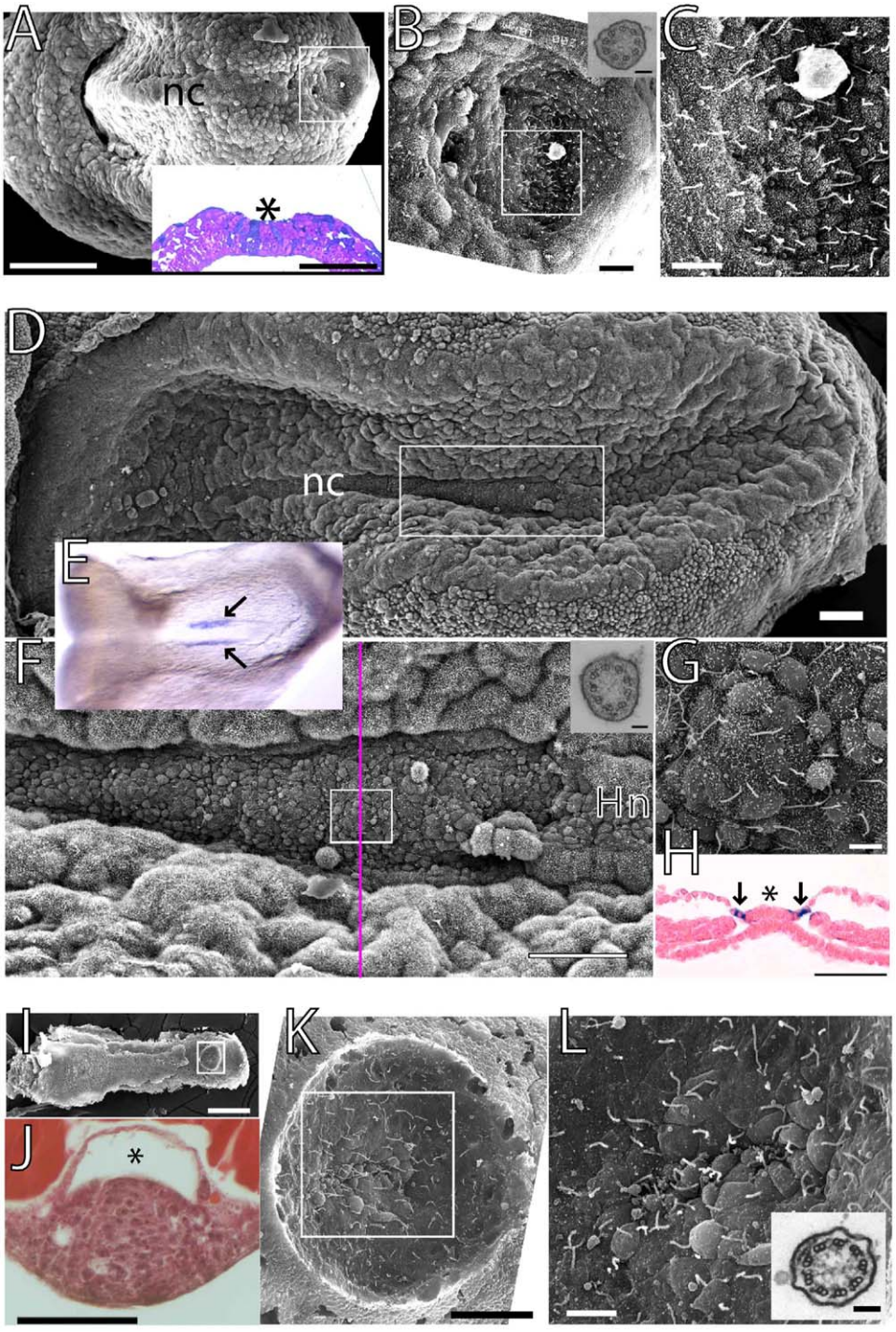

Figure 1. Morphology of the Ventral Node

Ventral nodes of the mouse (A–C), rabbit (D–H), and medakafish (I–L) are shown. All panels except for the transverse or crosssections are shown with the anterior side (head) on the left and the posterior side (tail) on the right. (A)–(C), (E)–(G), and (I)–(L) show ventral scanning electron microscope views. The white rectangle region is magnified in the next view. Notochord is indicated by "nc." Hn shows the position of the Hensen's node. Light microscope images of transverse sections of the ventral node (*) are also shown in (A), (H), and (J). Crosssections of the cilia are also shown in (B), (F), and (L). Expression of *nodal* (arrows) is shown by whole-mount in situ hybridization in (E) and (H). Bars: (A), 100 μm; (A) inset, 50 μm; (B), 10 μm; (B) inset, 0.1 μm; (C), 5 μm; (D), 100 μm; (F), 100 μm; (F) inset, 0.1 μm; (G), 5 μm; (H)–(J), 100 μm; (K), 50 μm; (L), 5 μm; and (L) inset, 0.1 μm.

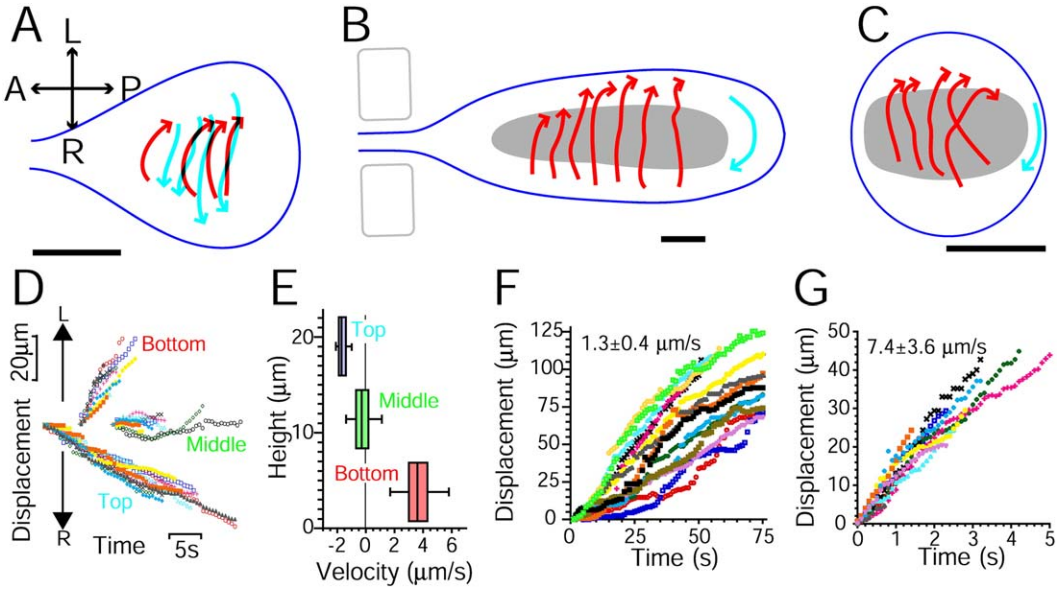

Figure 2. Leftward Flow in the Ventral Node

Flow was measured from the trajectories of exogenously introduced latex beads or endogenous debris in the ventral node of the mouse (A, D, and E), rabbit (B and F), and medakafish (C and G). (A)–(C) show the traces of latex beads (red, rapid leftward flow; cyan, slower counterflow). The edges of the ventral nodes are shown by the blue lines, and the gray regions in (B) and (C) show the uplift of the surface (see Movies S1–S6). Bars, 50 μm. (D), (F), and (G) show the traces of the displacement of the probe for the flow (exogenously introduced latex beads or endogenous debris). (E) shows the box-and-whisker plot of the velocity of the flow plotted against the height from the bottom surface of the nodal pit of the mouse.

nearly circular, especially when observed from the direction nearly parallel to the circulating axis of the ciliary movement (Okada et al., 1999). When the nodal cilium was observed from the direction perpendicular to the nodal cell layer, the trajectory of its tip was mostly elliptic, with the center located more posteriorly than the root of the cilium (Figures 3A–3C). This elliptic trajectory is the projection of the circular trajectory in the real three-dimensional space to the imaging plane parallel to the nodal cell layer. Thus, from this elliptic trajectory, we can estimate the direction of the axis around which the cilium is circulating (Figure 3D and see Experimental Procedures for detail).

This analysis quantified that cilia move around an axis tilted 40° ± 10° (0° = normal to the cell surface) to the posterior (180° ± 40°, 0° = anterior) (Figure 3E). The slant height of the conic rotation estimated from the fitting (ρ, Figure 3F) was significantly longer than the length of the cilium measured from the SEM micrographs (Figure 1). This might be due to the shrinkage and break during the electronmicroscopy process. The nodal cilia always appear much longer with living samples than those fixed and processed for immunostaining and/or electronmicroscopy. It should also be noted that this parameter does not directly indicate the actual length of the cilium, because the nodal cilium is not rotating as a rigid body but is slightly bent due to the viscosity of the surrounding fluid. The relatively large variance in the estimated value of this parameter will reflect the variance in the bending of each cilium. The estimated apex angle of the conical movement of the cilium (Ψ, Figure 3G) was consistent with the geometrical constraint: $\Theta+\Psi < 90°$. The sum and the difference of these angular parameters were $\Theta + \Psi \sim 90°$ and $\Theta - \Psi \sim 0°$.

The average length of cilia and the frequency of circular motion were different among the vertebrate species under study, but the dynamics of the cilia appeared similar, as summarized in Figure 3I. This evolutionarily conserved similarity in the ciliary dynamics suggests their importance in the production of the leftward flow. The clockwise motion around an axis tilted posteriorly by 40° and with the apex angle of approximately 40° (Figures 3E and 3G) results in a leftward swing of the cilium while it is extended nearly vertically. Because this motion is occurring far away from the surface, this part of the cycle is most effective in producing a leftward flow and can be referred to as the "effective stroke." In the other half of the cycle, which can be referred to as the "recovery stroke," the cilium sweeps rightward, close to the cell surface. Hydrodynamics show that a stationary surface retards the movement of nearby fluid. This makes it difficult for a cilium to move fluid when it is close to a surface and also increases the resistance to movement of the cilium, which may, as in the examples seen here, reduce the angular velocity during the recovery stroke. This surface effect is widely exploited by cilia to enhance the difference in flow created by effective and recovery strokes, resulting in net flow in one direction (Blake and Sleigh, 1974).

A Posteriorly Shifted Position of the Basal Body Might Determine the Posteriorly Tilted Axis of the Rotation-Like Beating of Cilium

Our analysis thus demonstrated that the nodal cilia moves around the posteriorly tilted axis. By reviewing

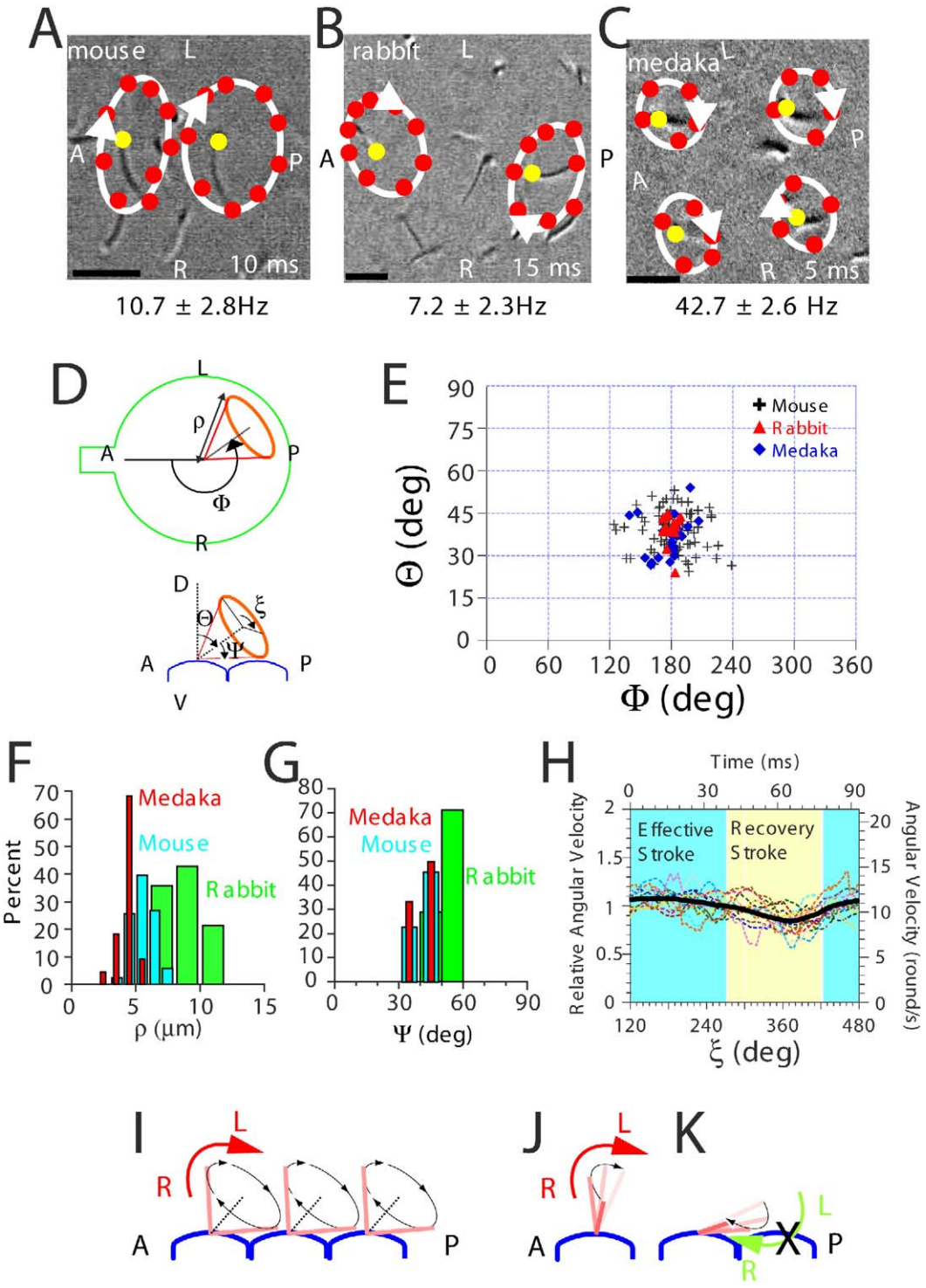

Figure 3. Posteriorly Tilted Rotation-Like Beating of the Cilia

(A–C) Traces of the cilia. Orientation, the species of the animal, the time interval of the trace, and the frequency of the beating are indicated in the figure. Red circles show the position of the end of the cilia at each time point, and the yellow circles show the position of the root of the cilia. White ellipses show the trajectory of the tip. In these panels, only cilium with its root well separated from the trajectory of the tip is presented for better reproduction. See Movies S6–S9 for representative cases, in which the root of the cilium is much closer to the anterior end of the trajectory of the tip. Bars, 5 μm.

(D–H) Quantitative analysis of cilia movement. (D) Definition of the analysis parameters. The circular movement of the tip of cilium is parameterized with the following parameters: the tilting of the axis of rotation Θ, the direction of the axis Φ, the slant height of the conic rotation of the ciliary tip ρ, and the apex angle of the conic rotation of the cilia Ψ. The distribution of these parameters are plotted in (E)–(G). (H) Angular velocity on the estimated circular trajectory plotted against the phase ξ (mouse).

(I) Schematic representation of results shown in (E)–(H). The three-dimensional movement of the cilia is schematically shown to reflect the average of the parameters of the ciliary movement plotted in (E)–(H).

(J and K) A hydrodynamic mechanism reinforces the beating dynamics with leftward power stroke. See text for details.

the SEM images in light of this finding, we noticed that most of these cilia project from the posterior side of the apical plasma membrane (Figure 4B). To confirm this posterior projection of nodal cilia, we examined the position of the basal body in the monociliated cells in the rabbit embryo, whose flat and large ventral node allows easier visualization. Immunofluorescent staining of the basal body (Figure 4A) clearly demonstrated that nearly 70% of the basal bodies were found near the posterior end of the apical dome-like surface of the monociliated cells. Some basal bodies were near the center of the apical dome, but very few were found on the anterior side.

This posterior positioning of the basal body in the monociliated cell might reflect the anterior-posterior polarity. Such planar cell polarity of the epithelial cell sheet is known to play important roles in developmental processes (Fanto and McNeill, 2004). Although it is not clear how the positioning of the basal body is shifted to the posterior side, this posterior shifting will result in the posteriorly tilted projection of the monocilia. The beating axis of monocilium might be determined as normal to the plasma membrane. Then, the posteriorly shifted positioning of the root of the monocilium along with the dome-like curvature of the ventral, apical plasma membrane can potentially explain the posterior tilting of the axis of its circling movement. This ventro-posterior projection of the monocilium will determine its rotation axis, and the hydrodynamic mechanism, as discussed above, will convert the rotation-like movement around this axis into the unidirectional leftward flow of the surrounding fluid.

Disordered Arrangement of the Rotating Axis of Cilia Leads to the Slow and Meandering Flow in *inv* Mutant Mouse Embryos

We have further confirmed this model by examining *inv* mutant mouse embryos. The fluid in the nodal pit of the *inv* mouse flows slowly to the left, but the streamline is meandering (Okada et al., 1999). If the tilting of the axis of the circling movement of cilia determines the directionality of the flow, the meandering streamline of the *inv* mutant might be resulting from the larger variance in the direction of the tilting. To examine this, we have examined the ciliary dynamics in *inv* mutant mouse embryos (Movie S10) and measured the tilting of the beating axis of cilia of both *inv*/*inv* mutant embryos and *inv*/+ heterozygous control embryos. As shown above, the axis of circling movement of almost all cilia of +/+ wild-type embryos are tilted to the posterior (Figure 3E). With *inv*/*inv* mutant embryos, nearly 20% of the cilia are anteriorly tilted, though the majority of cilia are posteriorly tilted (Figures 5A and 5B). The phase and the direction of the effective and recovery stroke of these anteriorly tilted cilia are reversed. They swing rightward when they are extended nearly vertically and sweep leftward close to the cell surface (Figure 5C). The heterozygous embryos showed a phenotype in-between; the variance of the distribution of the tilting direction is larger than wild-type, but no anteriorly tilted cilia were observed with heterozygous embryos. We have also noted that the circling movement of the cilium itself is partially affected by the mutation. In wild-type embryos, nearly 90% of cilia are rapidly circling in a clockwise direction, and immotile cilia are less than 10% at the bottom of the ventral node, as observed in this study. On the contrary, about 30% of heterozygous cilia and about half of mutant cilia were immotile or very slow. We have also found that some (typically one to five for each node) cilia of mutant embryos are circling in the reverse direction (counterclockwise). Thus, the slow and meandering flow of *inv* mutant embryos will be caused by the disordered arrangement of the rotating axis of cilia and by the aberrant rotation of cilia itself. This gives experimental support for our model that the posteriorly tilted, clockwise rotation of cilia produces the leftward flow. These results also suggest that the *inv* mutation might affect the alignment of nodal pit cells along the anterior-posterior axis (for example, planar cell polarity) as well as the movement of cilia.

The Leftward Flow Can Form the Concentration Gradient of Protein in the Ventral Node

Although the rapidly nonplanar beating dynamics of cilia and leftward flow of the fluid are conserved, the size and shape of the ventral node and the velocity of the flow are very different among these species. Flow velocity is much slower in the rabbit, while the size of the ventral node of the rabbit is much larger. Thus, we have underscored whether these different leftward flows are able to induce a protein gradient. Importantly, it should be noted that the Peclet number, a dimensionless parameter of the significance of the advection of the flow over diffusion, is conserved for the three species analyzed in this study (see Supplemental Data). Specifically, the product of the width of the ventral node and the flow velocity ranged within 1.5 to 2 × 10^{-6} cm^2/s. This conserved value is theoretically large enough for the flow to dominate over diffusion of proteins with molecular weights above 20 kDa that have diffusion coefficients up to ~1 × 10^{-6} cm^2/s and, consequently, to allow the appearance of protein gradients.

To clarify this issue, we have directly examined whether the flow can generate a concentration gradient of protein by measuring the distribution of fluorescently labeled protein locally produced by the photolysis of the caged-fluorescein moiety. When the caged-fluorescently labeled dextran (equivalent to a 40 kDa protein) was released by transient local UV illumination (1 s) over the midline ridge or in the right-side furrow of the ventral node of rabbit embryos, it flowed to the left side and then remained for more than 2 min in the left furrow (Figure 6A, Movie S11). As expected, smaller molecules (3 kDa dextran, equivalent to a 10 kDa protein) rapidly diffused after the photolysis over the midline ridge and was symmetrically distributed in both the left and right furrows (movie not shown). The long retention of dextran in the furrow could be due to stagnated flow by the less motile or immotile cilia on the surface in the furrow.

This furrow-like structure is missing in the murine nodal pit. The transiently released protein (with large molecular weights above 20 kDa) flowed to the left side as observed in the rabbit embryo, but it did not appear to stay on the left edge (Figure S1). The fluorescent signal became undetectable within a few seconds. On the

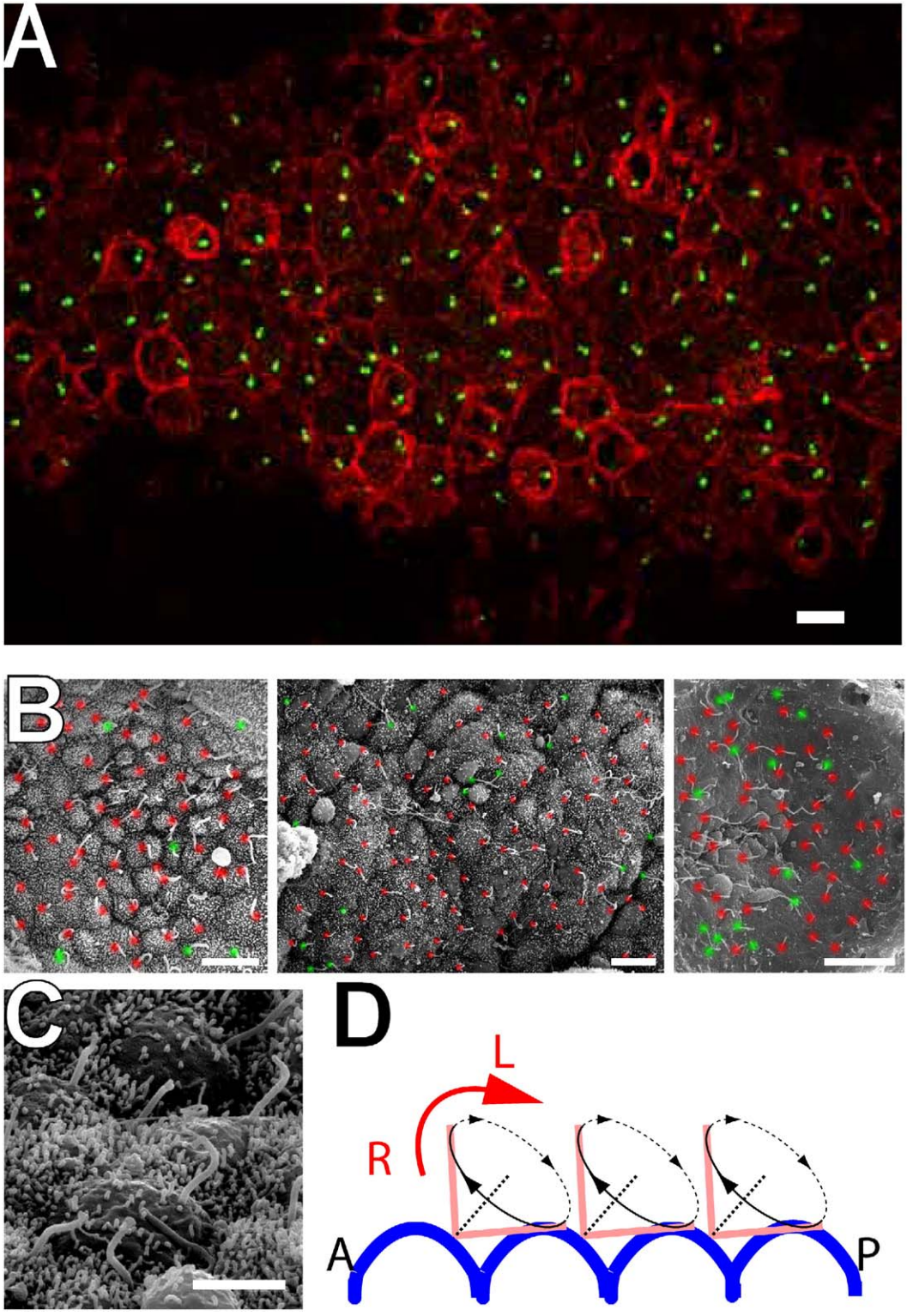

Figure 4. Ventro-Posterior Projection of Monocilia by the Posteriorly Positioned Basal Body

All micrographs and schema are shown with the anterior side on the left.

(A) This panel shows the optically sectioned image of the ventral node of the rabbit embryo. Basal body is stained with anti-γ-tubulin antibody in green, and the cell surface is stained with anti-rabbit antibody in red. Bar, 10 μm.

(B) SEM micrographs of ventral nodes of mouse (left), rabbit (middle), and medaka (right). Roots of cilia are colored red when they are located in the posterior side of the apical cell surface, and otherwise they are colored green. About 85% of cilia are projected from the posterior side of the nodal cell (245/302 in mouse, 809/882 in rabbit, and 115/156 in medaka). Bars, 10 μm.

(C) Higher magnification SEM micrograph of rabbit nodal ciliated cells. Note the dome-like curvature of the apical plasma membrane and the posteriorly tilted projection of the monocilia nearly perpendicular to the plasma membrane. Bar, 5 μm.

(D) Schematic representation of the ventro-posterior projection of monocilia.

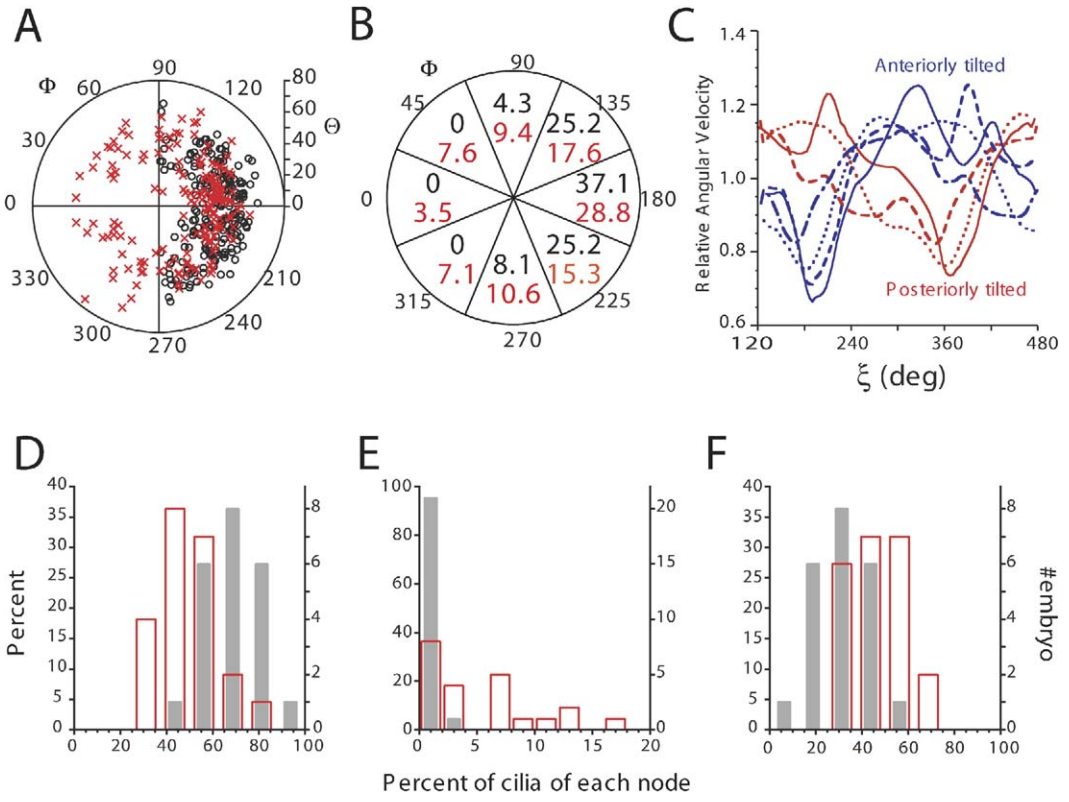

Figure 5. Disorganized Alignment of the Tilting Axis of Ciliary Beating in the *inv* Mutant Mouse

(A and B) Distributions of the tilting of the rotation axis Θ and the direction of the axis Φ (A). Numbers show the percentages of the cilia tilting to the direction of each sector (B, n = 210 cilia from 22 embryos for *inv*/+ [black] and 170 cilia from 22 embryos for *inv/inv* [red]). There was a significantly larger variance in Φ in the *inv/inv* mutant (*var* [Φ] = 1800 for *inv*/+ and 6000 for *inv/inv*, $p < 10^{-16}$ by F test), but there was no significant difference between the means (<Φ> = 183 for *inv*/+ and 181 for *inv/inv*).

(C) Angular velocity of the tip of the cilia of the *inv/inv* mutant embryos plotted against the phase ξ as in Figure 3H. Red traces show the velocity profiles of the posteriorly tilted cilia, and blue traces show those of the anteriorly tilted cilia.

(D–F) Distribution of the frequency of clockwise rotation (D), counterclockwise rotation (E), and immotile cilia (F). For each panel, the difference of distribution between *inv*/+ (black) and *inv/inv* (red) embryos (22 embryos each) was statistically significant ($p < 10^{-5}$ by t test, and $p < 10^{-3}$ by Kolmogolov-Smirnov test).

contrary, the continuous release by weak UV illumination resulted in the stationary L-R asymmetric distribution of proteins with molecular weights of 20–40 kDa (Figures 6B, 6C, and 6E, Movie S12). The fluorescent signal in the left and right regions reached stationary level within 1 to 2 min, and the asymmetric distribution remained stationary for the duration of the observation (Figure S4). The larger molecules, even though they diffuse more slowly, showed less asymmetric distribution (Figures 6D and 6E, Figures S3A and S3B, Movie S13, seeSupplemental Data for further theoretical discussion). The smaller molecules diffuse so rapidly that transport by the leftward flow is not noticeable, and they can only reach a symmetric distribution (Figure 6E, Supplemental Data, Movie S14). These results show that, with both rabbit and mouse embryos, proteins ~40 kDa that are secreted into the ventral node will be asymmetrically distributed. Therefore, the flow is fast enough for the generation of a concentration gradient of putative morphogenic proteins with highest concentration on the left side. One might argue that the left-right difference in the stationary distribution measured here will be too small to trigger the stable asymmetric gene expression. However, the magnitude of the left-right difference depends on many parameters, such as the size of the secretion area, rate of secretion, and rate of degradation or inactivation. For example, our in silico simulation confirmed a theoretical prediction that faster degradation or inactivation generates steeper gradient (Figure S3B). Our experiment also suggests another possibility, that repetitive intermittent release and temporal integration might enable large and stable response (Figure S3C).

Relation of Our Hydrodynamic Model to the Previous Experimental Results

A previous paper suggested that a fast artificial flow to the left does not disturb development, while a fast artificial flow to the right can reverse situs (Nonaka et al. 2002). We believe that these results are consistent with the morphogen gradient model. Although it seems that a fast leftward flow might wash away a morphogen, we believe that the flow rate is not fast enough to do so. For a quantitative discussion of this issue, please see Supplemental Data. We propose that a secreted factor, if released continuously with faster

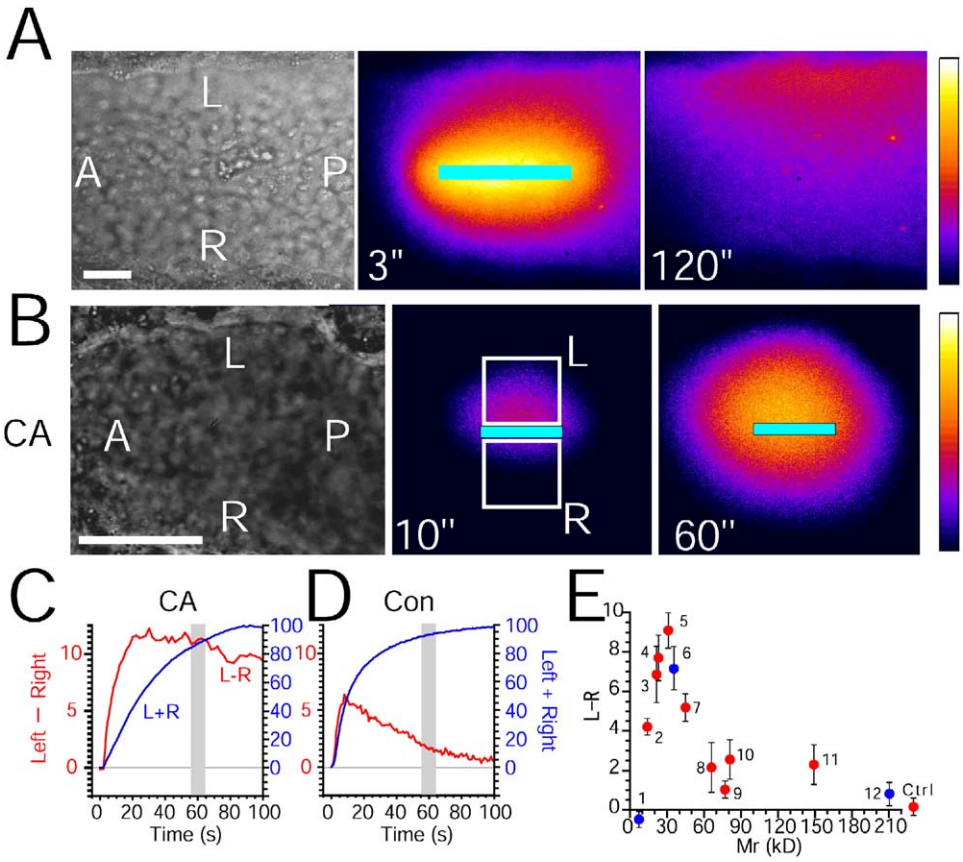

Figure 6. Distribution of the Exogenously Introduced Proteins in the Ventral Node

(A) Asymmetric distribution of the caged fluorescently labeled dextran (equivalent to a 40 kDa globular protein [Experimental Procedures]) in the rabbit embryo after transient photo release. A bright field image and pseudocolored fluorescent images 3 s and 120 s after a 1 s photo release over the midline (cyan bar) are shown.

(B) Distribution of continuously photo-released proteins in the mouse embryo. Results with carbonic anhydrase (molecular weight = 31 kDa) are shown. Bright field images and fluorescent images after 10 s and 60 s from the initiation of the continuous photo release at the midline (cyan bars) are shown.

(C and D) Time course of the asymmetric distribution of the protein in the experiment with carbonic anhydrase ([B], molecular weight = 31 kDa) and with conalbumin (Figure S3A, molecular weight = 77 kDa). Fluorescent intensities in boxes L and R were measured, and their sum (L+R) and difference (L–R) are plotted. The fluorescent intensity was normalized by the maximum intensity so that the axes show the values in arbitrary fluorescence unit.

(E) The L–R difference in the stationary phase (average of 55–65 s after photo release, gray in [C]). The mean (circle) and standard error (error bar) are plotted against molecular weight. Red circles show the results with protein, and blue circles show the results with dextran. For the comparison with the data with globular proteins, data with dextran are plotted by the molecular weight of globular protein with the same diffusion coefficient. Key: 1, dextran (3 kDa); 2, soybean trypsin inhibitor; 3, RNase A; 4, chymotrypsinogen; 5, carbonic anhydrase; 6, dextran (10 kDa); 7, ovalbumin; 8, bovine serum albumin; 9, conalbumin; 10, transferrin; 11, aldolase; 12, dextran (70 kDa); and ctrl, control (carbonic anhydrase without embryo).

flow, will be more likely to form a steady L-R asymmetric gradient with higher concentration on the left, since advection by faster flow will dominate diffusion. Thus, both artificial slow and fast leftward flow can create asymmetric distributions of secreted factors and elicit normal situs. Furthermore, Watanabe et al. (2003) showed that laterality defects in *inv* mutants were corrected by an artificial fast leftward flow. This is also consistent with the morphogen model, which indicates that not only the direction of the flow is important (wild-type and *inv* mutants both have leftward flows) but the speed of the flow is also essential to fix the proper L-R asymmetry.

Thus, our results and others' are consistent with our morphogen gradient model, but this does not exclude other possible mechanisms. For example, morphogen gradients specifying positional information in the embryo have been proposed to arise by diffusion and by transport involving exocytosis and endocytosis of membrane carriers, such as argosomes and exosomes (González-Gaitán, 2003). The leftward flow will efficiently transport small membrane carriers to the left like the plastic beads used in this and previous studies (Nonaka et al., 1998; Okada et al., 1999). As suggested previously, the immotile subpopulation of the nodal cilia, which are more abundant near the edges of the ventral node, might serve as the sensor for the concentration gradient of the morphogen. The flow itself could also mechanically stimulate these immotile cilia (Tabin and Vogan, 2003; McGrath et al., 2003).

In summary, our results give a detailed description of the ciliary and flow dynamics in three different vertebrate species, pointing out the conserved features relevant for further understanding of the mechanisms involved in L-R axis determination. Our results indicate that all species under study show a leftward flow in their ventral nodes. In all cases, cilia have nonplanar leftward beating dynamics, as proposed from mathematical modeling and in silico experiments (J. Buceta, M. Ibañes, D. Rasskin-Gutman, Y.O., N.H., and J.-C.I.B., unpublished data). The information of the A-P and D-V axes is integrated into the configuration of the cilia; they project ventrally and their motion is tilted posteriorly, such that asymmetric ciliary left-right dynamics arises. Chirality is implemented as the chiral structure of the axoneme, which in turn could determine the clockwise direction of the rotation-like beating. The information on the A-P and D-V axes and the chirality seems, thus, to be integrated and converted into L-R asymmetric dynamics at the level of each single cell (cilium), as expected from the conceptual model of the chiral F molecule (Brown and Wolpert, 1990). Thus, the fluid flow may translate the left-right asymmetry at the cellular level to the L-R embryonic axis by defining, through the asymmetric concentration of a morphogen, which side of the node is the left and which side is the right. Furthermore, cilia sweep just above the apical surface of the ciliated cell during their recovery stroke. This sweep might also facilitate the release of the putative morphogen bound to the lipid membrane or extracellular matrix. Finally, we have shown that the leftward flow of fluid is fast enough to generate the concentration gradient of the putative proteinous morphogen, and we have characterized under which conditions such a gradient can emerge. Future studies on putative morphogens will clarify the mechanism that determines the L-R axis information conveyed by the flow.

Experimental Procedures

Reagents

Culture media were obtained from Invitrogen (Carlsbad, CA). Other reagents were obtained from Wako Pure Chemical Industries (Chuo-ku, Osaka, Japan) unless otherwise stated.

Electron Microscopic Observation of Embryos

Electron microscopy of mouse and rabbit embryos were performed according to the previous study (Takeda et al., 1999). For medakafish embryos, we used a partially modified protocol (addition of 0.5% tannic acid) (Takeda et al., 1995). Scanning electron microscopy for all three species was carried out as described previously (Takeda et al., 1999).

Whole-Mount In Situ Hybridization

Whole-mount in situ hybridization was performed with a standard method as described previously (Takeda et al., 1999). Briefly, rabbit embryos were fixed for 12–36 hr at 4°C with 4% paraformaldehyde (Merck) in PBS (Sigma), hybridized with a DIG-labeled RNA probe transcribed from mouse *nodal* cDNA (kindly provided by Dr. Hamada [Osaka University]), and an alkaline-phosphatase-conjugated anti-DIG antibody (Roche). Following development of color, 10 μm thick paraffin sections were made and counterstained with EosinY.

Enhanced Video Microscopic Observation of Mouse Embryos

The embryos of timed pregnant ICR mice (CLEA Japan, Meguro-ku, Tokyo, Japan) were dissected and mounted on a silane-coated glass slide with a silicone rubber spacer, as described previously (Okada et al., 1999). Only embryos with a fully developed node (nodal stage 5 or 6 [Okada et al., 1999]) were selected for the analysis. Fluorescent beads (1 μm diameter, carboxylate-modified microspheres, Molecular Probes) were added to the DR50 medium (DME supplemented with 50% rat serum and 10 μM sodium pyruvate). An Olympus (Chiyoda-ku, Tokyo, Japan) BX-51WI microscope with an Olympus UPlanApo 60×/1.20 w objective was used. A fluorescent image of the beads and the differential interference contrast (DIC) image of the embryo were simultaneously taken with a Neptune CCD camera (Watec, Tsuruoka, Yamagata, Japan) with a 2 ms electric shutter. For high-speed recording, the DIC image was recorded with a high-speed CCD camera, HG Imager 2000 (Eastman Kodak, Rochester, NY) at 500 frames per s. The genotype of mutant mouse embryos was determined after observation, as described previously (Okada et al., 1999).

Observation of Rabbit Embryos

Embryos were obtained from timed pregnant rabbits (Japan White, Kitayama Labes, Ina, Nagano, Japan). The embryos were dissected and mounted in a custom-made glass-bottom dish (Matsunami, Kishiwada, Osaka, Japan). The discoid embryos were immobilized by two strips of cover glass (0.2 mm thickness, Mastumani) put on the right and left extraembryonic region. The embryo was maintained in the medium (Ham's F10 medium supplemented with 10% rabbit serum) in which fluorescent beads were added for visualization of flow. An XLUMPlanFI 20×/0.95 w objective (Olympus) and a Neptune CCD camera were used for observation of the flow, and a UPlanApo 60×/1.20 w objective and HG Imager 2000 were used for the observation of cilia movement.

Observation of Medakafish Embryos

Fertilized eggs of wild-type medakafish (a generous gift from Drs. Shimada, Aizawa, and Shima [University of Tokyo]) were maintained at 24°C. The embryos were dechorionated with hatching enzyme (a generous gift from Dr. Yasumasu [Sophia University]; Yasumasu et al. [1992]) and mounted on a glass slide with a silicone rubber spacer. A UPlanApo 60×/1.20 w objective was used with a Neptune camera or an HG Imager 2000.

Immunofluorescent Staining of Rabbit Embryos

Rabbit embryos were dissected and maintained as above before fixation with cold methanol at –20°C. Embryos rehydrated with PBS supplemented with 1% Triton X-100 were incubated with anti-γ-tubulin antibody GTU-88 (Sigma) in PBS supplemented with 0.05% Tween 20 and 5% FBS. After thorough washing, embryos were stained with AlexaFluor488-labeled anti-mouse antibody and AlexaFluor555-labeled anti-rabbit antibody (Invitrogen). Embryos were mounted in PBS containing 1 μM DRAQ5 (Alexis). Samples were observed with EC PlanNeofulor 40× objective on Axio Imager (Zeiss), and optically sectioned images were obtained with ApoTome and AxioCam MRm CCD camera (Zeiss).

Analysis of Cilia Movement

The digitized images of the high-speed CCD camera were analyzed with NIH Image software (a free software developed at the National Institutes of Health). The axial resolution of our high numerical aperture DIC system is about 0.7 μm, which enabled the selection of the region of the ventral node vertical to the optical axis. Typically, an area of about 20 μm × 20 μm at the bottom of the ventral node in the same optical plane was observed so that the optical axis is aligned within 0.7/10 radian = 4° to the axis perpendicular to the nodal cell layer in the observation area. The tip and root of each cilium were traced in each video frame. The vector from the root to the tip was expressed by the polar coordinate as (r, θ) and plotted. The power spectrum of the polar angle θ was estimated by Berg's Maximum Entropy Method for analysis of beating frequency (Nakata et al., 1993). For estimating parameters of the conic movement, vector coordinates were fitted to the theoretical ellipse (see below):

$$\frac{\{r\cos(\theta-\Phi)-\rho\cos\Psi\sin\Theta\}^2}{(\rho\sin\Psi\cos\Theta)^2}+\frac{\{r\sin(\theta-\Phi)\}^2}{(\rho\sin\Psi)^2}=1$$

where ρ, Θ, Φ, and Ψ are the parameters indicated in Figure 3D. The fitting was performed with a software package, Origin 7 (Origin Lab, Northampton, MA). The back projection of the elliptic trajectory was calculated by the following:

$$x = \frac{r\cos(\theta - \Phi) - \rho\cos\Psi\sin\Theta}{\cos\Theta}, \quad y = r\sin(\theta - \Phi)$$

Phase ξ was determined by

$$\xi = \tan^{-1}(y/x),$$

and the angular velocity was calculated by differentiating the phase ξ by time.

Measurement of the Distribution of Caged Fluorescently Labeled Protein

The following proteins were labeled with 5-carboxyfluorescein-bis-(5-carboxymethoxy-2-nitrobenzyl) ether, -alanine-carboxamide, succinimidyl ester (CMNB-caged carboxyfluorescein, SE, Molecular Probes): RNase A (14 kDa, 13 × 10^{-7}cm^2/s), soybean trypsin inhibitor (21.5 kDa, 10 × 10^{-7}cm^2/s), bovine chymotrypsinogen A (23 kDa, 9.5 × 10^{-7}cm^2/s), carbonic anhydrase (31 kDa, 11 × 10^{-7}cm^2/s), ovalbumin (45 kDa, 8.1 × 10^{-7}cm^2/s), bovine serum albumin (66 kDa, 6.5 × 10^{-7}cm^2/s), conalbumin (77 kDa, 6.3 × 10^{-7}cm^2/s), bovine transferrin (81 kDa, 6.2 × 10^{-7}cm^2/s), and aldolase (149 kDa, 4.6 × 10^{-7}cm^2/s). Ten milligrams of protein were reacted with 1 mg caged-fluorescein reagent in 0.1 M phosphate buffer at pH 7.5 for 1–2 hr at 37°C, and the free dye was removed by gel filtration through a NAP-5 column (Amersham). The buffer was exchanged with the DME medium at the same time. The labeling was checked spectroscopically and by SDS-PAGE analysis. Caged-fluorescein-labeled dextran (3 kDa 22 × 10^{-7}cm^2/s, 10 kDa 9.1 × 10^{-7}cm^2/s, and 70 kDa 3.6 × 10^{-7}cm^2/s) was purchased from Molecular Probes. The labeled protein or dextran was added to the medium at ~0.1 mg/ml. The UV light for uncaging the cage moiety was focused to the 20 μm × 1 μm area with the XLUMPlanFI 20×/0.95 w objective or the UPlanApo 60×/1.20 w objective by projecting the image of the slit (Sigma Koki, Sumida-ku, Tokyo) on the back focal plane. The slit, filters, and a shutter (Sigma Koki) were set to the custommade illumination tube. Blue excitation light for fluorescent observation of the uncaged protein was simultaneously introduced to the epifluorescent illumination light path by another custom made illumination tube so that the uncaged protein could be simultaneously observed during the uncaging. For the measurement of steady-state distribution, the UV light attenuated by two successive ND filters (50% and 10%) continuously illuminated the midline area of the sample. For measurement of the distribution of transiently uncaged protein, the protein was uncaged by 1 s (for rabbit) or 1/8 s (for mouse) illumination of the nonattenuated UV light through the same slit. The distribution of uncaged protein was observed with a Neptune CCD camera with a 1/15 s exposure, and the digitized image was analyzed with NIH Image software. To avoid the adverse effect of free radicals formed by the uncaging photochemical reaction, 2-mercaptoethanol was added to the DR50 medium as a scavenger. The viability of the embryos was assessed before and after the experiment by the movement of the cilia.

Supplemental Data

Supplemental Data include three figures, text, and Supplemental References and can be found with this article online at http://www.cell.com/cgi/content/full/121/4/633/DC1/.

Acknowledgments

We thank Masato Ohta and Kazuhiro Eto for technical advice on manipulation of mouse embryos; Hidetaka Kosako and Kenji Shimamura for technical assistance on manipulation of chick embryos; Hiroshi Hamada for the gift of the *nodal* probe; Atsuko Shimada, Kouichi Aizawa, Hiroshi Mitani, and Akihiro Shima for the gift of medakafish embryos; Naoto Matsuda and Masayoshi Mishina for the gift of zebrafish embryos; Shigeki Yasumasu for the hatching enzyme; Tomohiro Furukawa and Katsuyuki Abe for assistance in the design of the microscope; and Bruene Venus for AxioImager and Apotome. We also thank Daisuke Furihata, Hisashi Okamoto, Naoto Nagaosa, and Seiji Miyashita for the stimulating discussions on the hydrodynamic aspects of this phenomenon at the earliest stage of this project; Javier Buceta and Diego Rasskin-Gutman for the constructive comments on this manuscript; and Marta Ibañes for the revision, comments, and all the numerical analyses of the distribution of proteins shown in the Supplemental Data. Part of the results (posteriorly tilted rotation-like beating of cilia) of this paper was presented in the annual meetings of the Japanese Association for Anatomists in 2002 and 2003, International Meeting of the Interest Group for Cilia, Mucus and Mucociliary Interactions supported by the PCD Foundation held in Miami in 2002 and in the annual meeting of the Japan Society for Cell Biology in 2003. This work was supported by a Center of Excellence Grant-in-Aid from the Ministry of Education, Science, Sports, and Culture of Japan to N.H. and by the National Institutes of Health to J.-C.I.B.

Received: December 17, 2004
Revised: January 28, 2005
Accepted: April 5, 2005
Published: May 19, 2005

References

Amack, J.D., and Yost, H.J. (2004). The T box transcription factor no tail in ciliated cells controls zebrafish left-right asymmetry. Curr. Biol. *14*, 685–690.

Bellomo, D., Lander, A., Harragan, I., and Brown, N.A. (1996). Cell proliferation in mammalian gastrulation: the ventral node and notochord are relatively quiescent. Dev. Dyn. *205*, 471–485.

Bisgrove, B.W., and Yost, H.J. (2001). Classification of left-right patterning defects in zebrafish, mice, and humans. Am. J. Med. Genet. *101*, 315–323.

Blake, J.R., and Sleigh, M.A. (1974). Mechanics of ciliary locomotion. Biol. Rev. Camb. Philos. Soc. *49*, 85–125.

Brown, N.A., and Wolpert, L. (1990). The development of handedness in left/right asymmetry. Development *109*, 1–9.

Cartwright, J.H., Piro, O., and Tuval, I. (2004). Fluid-dynamical basis of the embryonic development of left-right asymmetry in vertebrates. Proc. Natl. Acad. Sci. USA *101*, 7234–7239.

Essner, J.J., Vogan, K.J., Wagner, M.K., Tabin, C.J., Yost, H.J., and Brueckner, M. (2002). Conserved function for embryonic nodal cilia. Nature *418*, 37–38.

Fanto, M., and McNeill, H. (2004). Planar polarity from flies to vertebrates. J. Cell Sci. *117*, 527–533.

González-Gaitán, M. (2003). Signal dispersal and transduction through the endocytic pathway. Nat. Rev. Mol. Cell Biol. *4*, 213–224.

Hirokawa, N. (2000). Stirring up development with the heterotrimeric kinesin KIF3. Traffic *1*, 29–34.

Lowe, L.A., Supp, D.M., Sampath, K., Yokoyama, T., Wright, C.V., Potter, S.S., Overbeek, P., and Kuehn, M.R. (1996). Conserved left-right asymmetry of nodal expression and alterations in murine situs inversus. Nature *381*, 158–161.

McGrath, J., Somlo, S., Makova, S., Tian, X., and Brueckner, M. (2003). Two populations of node monocilia initiate left-right asymmetry in the mouse. Cell *114*, 61–73.

Mercola, M., and Levin, M. (2001). Left-right asymmetry determination in vertebrates. Annu. Rev. Cell Dev. Biol. *17*, 779–805.

Nakata, T., Sato Yoshitake, R., Okada, Y., Noda, Y., and Hirokawa, N. (1993). Thermal drift is enough to drive a single microtubule along its axis even in the absence of motor proteins. Biophys. J. *65*, 2504–2510.

Nonaka, S., Tanaka, Y., Okada, Y., Takeda, S., Harada, A., Kanai, Y., Kido, M., and Hirokawa, N. (1998). Randomization of left-right asymmetry due to loss of nodal cilia generating leftward flow of extraembryonic fluid in mice lacking KIF3B motor protein. Cell *95*, 829–837.

Nonaka, S., Shiratori, H., Saijoh, Y., and Hamada, H. (2002). Deter-

mination of left-right patterning of the mouse embryo by artificial nodal flow. Nature *418*, 96–99.

Okada, Y., Nonaka, S., Tanaka, Y., Saijoh, Y., Hamada, H., and Hirokawa, N. (1999). Abnormal nodal flow precedes situs inversus in *iv* and *inv* mice. Mol. Cell *4*, 459–468.

Supp, D.M., Brueckner, M., Kuehn, M.R., Witte, D.P., Lowe, L.A., McGrath, J., Corrales, J., and Potter, S.S. (1999). Targeted deletion of the ATP binding domain of left-right dynein confirms its role in specifying development of left-right asymmetries. Development *126*, 5495–5504.

Tabin, C.J., and Vogan, K.J. (2003). A two-cilia model for vertebrate left-right axis specification. Genes Dev. *17*, 1–6.

Takeda, S., Funakoshi, T., and Hirokawa, N. (1995). Tubulin dynamics in neuronal axons of living zebrafish embryos. Neuron *14*, 1257–1264.

Takeda, S., Yonekawa, Y., Tanaka, Y., Okada, Y., Nonaka, S., and Hirokawa, N. (1999). Left-right asymmetry and kinesin superfamily protein KIF3A: new insights in determination of laterality and mesoderm induction by kif3A$^{-/-}$ mice analysis. J. Cell Biol. *145*, 825–836.

Vogan, K.J., and Tabin, C.J. (1999). A new spin on handed asymmetry. Nature *397*, 297–298.

Wargo, M.J., and Smith, E.F. (2003). Asymmetry of the central apparatus defines the location of active microtubule sliding in Chlamydomonas flagella. Proc. Natl. Acad. Sci. USA *100*, 137–142.

Watanabe, D., Saijoh, Y., Nonaka, S., Sasaki, G., Ikawa, Y., Yokoyama, T., and Hamada, H. (2003). The left-right determinant Inversin is a component of node monocilia and other 9+0 cilia. Development *130*, 1725–1734.

Yasumasu, S., Yamada, K., Akasaka, K., Mitsunaga, K., Iuchi, I., Shimada, H., and Yamagami, K. (1992). Isolation of cDNAs for LCE and HCE, two constituent proteases of the hatching enzyme of Oryzias latipes, and concurrent expression of their mRNAs during development. Dev. Biol. *153*, 250–258.